



Gradients of column CO₂ across North America from the NOAA Global Greenhouse Gas Reference Network

Xin Lan^{1,2}, Pieter Tans¹, Colm Sweeney^{1,2}, Arlyn Andrews¹, Andrew Jacobson^{1,2}, Molly Crotwell^{1,2}, Edward Dlugokencky¹, Jonathan Kofler^{1,2}, Patricia Lang¹, Kirk Thoning¹, and Sonja Wolter^{1,2}

¹National Oceanic and Atmospheric Administration, Earth System Research Laboratory, Boulder, CO, USA

²University of Colorado, Cooperative Institute for Research in Environmental Sciences, Boulder, CO, USA

Correspondence: Xin Lan (xin.lan@noaa.gov)

Received: 30 March 2017 – Discussion started: 19 May 2017

Revised: 3 November 2017 – Accepted: 6 November 2017 – Published: 21 December 2017

Abstract. This study analyzes seasonal and spatial patterns of column carbon dioxide (CO₂) over North America, calculated from aircraft and tall tower measurements from the NOAA Global Greenhouse Gas Reference Network from 2004 to 2014. Consistent with expectations, gradients between the eight regions studied are larger below 2 km than above 5 km. The 11-year mean CO₂ dry mole fraction (XCO₂) in the column below ~330 hPa (~8 km above sea level) from NOAA's CO₂ data assimilation model, CarbonTracker (CT2015), demonstrates good agreement with those calculated from calibrated measurements on aircraft and towers. Total column XCO₂ was attained by combining modeled CO₂ above 330 hPa from CT2015 with the measurements. We find large spatial gradients of total column XCO₂ from June to August, with north and northeast regions having ~3 ppm stronger summer drawdown (peak-to-valley amplitude in seasonal cycle) than the south and southwest regions. The long-term averaged spatial gradients of total column XCO₂ across North America show a smooth pattern that mainly reflects the large-scale circulation. We have conducted a CarbonTracker experiment to investigate the impact of Eurasian long-range transport. The result suggests that the large summertime Eurasian boreal flux contributes about half of the north–south column XCO₂ gradient across North America. Our results confirm that continental-scale total column XCO₂ gradients simulated by CarbonTracker are realistic and can be used to evaluate the credibility of some spatial patterns from satellite retrievals, such as the long-term average of growing-season spatial patterns from satellite retrievals reported for Europe which show a larger spatial difference (~6 ppm) and scattered hot spots.

1 Introduction

Atmospheric measurements of carbon dioxide (CO₂) from ground and airborne platforms have greatly increased our knowledge of the global carbon cycle. Observations of CO₂, including the NOAA Global Greenhouse Gas Reference Network (GGGRN), initially emphasized ground-based measurements. These observations, started by C. D. Keeling, have monitored the CO₂ trend on both regional and global scales for over 50 years (e.g., Keeling and Rakestraw, 1960; Tans et al., 1989). In addition, the frequency and spatial distribution of airborne measurements have increased rapidly in the last two decades, providing important information about horizontal and vertical variability of atmospheric CO₂ (e.g., Gerbig et al., 2003; Choi et al., 2008; Biraud et al., 2013). Routine aircraft measurements from the NOAA/ESRL GGGRN monitor the large-scale distributions of a suite of trace gases, including CO₂, under the influence of continental processes (Sweeney et al., 2015). A very successful approach has been to employ commercial aircraft as a platform for CO₂ measurements, such as Japan's CONTRAIL (Comprehensive Observation Network for TRace gases by AirLiner) project, which has provided valuable information for CO₂ in the high troposphere and lower stratosphere (Machida et al., 2002, 2008). Vertical profiles of atmospheric CO₂ reflect the combined influences of surface fluxes and atmospheric mixing. Vertical profiles are particularly useful for evaluating vertical mixing in atmospheric transport models that are used for inverse modeling (e.g., Stephens et al., 2007) to derive estimates of regional-to continental-scale CO₂ sources and sinks (e.g., Tans et al., 1990; Gurney et al., 2002, 2004; Ciais et al., 2010).

While CO₂ sources and sinks are well constrained at the global scale by global mass balance, it remains challenging to accurately resolve CO₂ sources and sinks at regional to continental scale, the apportionment of which depends on relatively minor variations of the observed spatial and temporal patterns of CO₂. When averaging over a few months and longer, the largest portion of the variations over continents results from hemispheric-scale terrestrial uptake/emissions (photosynthesis/respiration) and fossil fuel emissions, while regional net fluxes can make a relatively small contribution to the signal. For example, a simple mass balance argument shows that all US CO₂ emissions from fossil fuel burning ($\sim 1.4 \text{ Pg yr}^{-1}$) create a total column enhancement of only 0.6 ppm on average in air parcels over the east coast compared to the west coast and Gulf Coast if we assume an average of 5 days for the winds to flush the contiguous US ($\sim 8 \times 10^{12} \text{ m}^2$).

With careful calibration, air handling, and analysis, the uncertainties of in situ measurements are less than 0.1 ppm. However, in situ observation networks are sparse in global and regional coverage. Remote sensing data radically increase the number of observations and capture undersampled regions. It could have a valuable impact on our understanding of the carbon cycle. However, both the precision and the potential of even very small systematic biases in remote sensing measurements need to be carefully evaluated, especially those that depend on regional and seasonal conditions. Vertical profiles from in situ CO₂ measurements have been used to evaluate ground-based total column XCO₂ (the “X” stands for dry mole fraction) determinations, such as those from the Total Carbon Column Observing Network (TCCON) (Washenfelder et al., 2006; Wunch et al., 2010; Messerschmidt et al., 2011; Tanaka et al., 2012). The uncertainty of TCCON total column CO₂ is reported to be 0.4 ppm (1σ) after comparison to aircraft measurements (Wunch et al., 2010). Vertical profiles are also used to evaluate other satellite retrievals of total column XCO₂, such as those from the Tropospheric Emission Spectrometer (TES) (Kulawik et al., 2013) and the Greenhouse Gases Observing SATellite (GOSAT) (Inoue et al., 2013, 2016; Saitoh et al., 2016). Satellite retrieval products have known and unknown biases (due to errors in spectroscopy, viewing geometry, spatial differences in clouds and aerosols, surface albedo, etc.) that can result in false horizontal gradients in total column XCO₂ for inverse estimates of sources (Miller et al., 2007; Crisp et al., 2012; Feng et al., 2016). After correction for known biases, the mean GOSAT total column CO₂ (National Institute for Environmental Studies – NIES – retrievals) biases range between -2.09 and 3.37 ppm (mean of 0.11 ppm, SD of 1.11 ppm; 20 out of 27 stations show biases lower than 1 ppm) across different aircraft sites over land when compared with aircraft-based total column XCO₂ (Inoue et al., 2016). The Orbiting Carbon Observatory 2 (OCO-2) retrieval of total column XCO₂ was estimated to have a mean difference less than 0.5 ppm from TCCON, with rms differences

typically below 1.5 ppm after bias correction (Wunch et al., 2017). The overall uncertainty of satellite retrievals is relatively large compared with the total column XCO₂ calculated from in situ measurements. Total column XCO₂ calculated from vertical profiles from the Japanese CONTRAIL project (Machida et al., 2008) and from the NOAA Carbon Cycle and Greenhouse Gas aircraft program (Sweeney et al., 2015) complemented with simulated profiles from a chemistry–transport model above the maximum altitude of the data have uncertainty less than 1 ppm (Miyamoto et al., 2013). The smaller uncertainty of the in situ based total column XCO₂ suggests that they can be used to evaluate satellite retrievals of column averaged CO₂. Since aircraft profiles co-located with satellite retrievals are rare, it is useful to consider the statistics of total column XCO₂ fields derived from repeated aircraft profiles over particular locations.

The effect of satellite column averaging kernels and a priori profiles when comparing aircraft-based column XCO₂ with GOSAT retrievals has been assessed by Inoue et al. (2013). For the case considered, application of the averaging kernel and a priori profile to simulate total column XCO₂ was generally within ± 0.1 ppm of the density-weighted total column, suggesting that the averaging kernels can only account for a small part of the overall uncertainty of the GOSAT total column XCO₂ (Inoue et al., 2013).

Transparent and objective estimates of CO₂ sources and sinks derived from atmospheric measurements are essential for validating emissions reduction efforts and other mitigation policies, and for lowering the uncertainties of carbon cycle–climate feedbacks. The latter are major ambiguities in predicting future climate, such as potential uncontrolled CH₄ and CO₂ emissions from warming permafrost in Arctic regions. Satellite retrievals of total column XCO₂ can significantly improve estimates of sources and sinks only if they are sufficiently precise and accurate (Houweling et al., 2004; Chevallier et al., 2014), meaning that even very small systematic errors (biases) must be eliminated. Here, we analyze the spatial and temporal variability of column CO₂ over North America using well-calibrated CO₂ measurements from aircraft and tall towers, and we use model results from NOAA’s CarbonTracker, version CT2015 (Peters et al., 2007, with updates documented at <http://carbontracker.noaa.gov>) to investigate the primary drivers of variability in total column XCO₂. The aircraft data enable direct analysis of column CO₂ characteristics, which is the fundamental step for accurate apportionment of sources and sinks. This study focuses on long-term averaged column CO₂ gradients and the contributions of different vertical layers to the total column variability. It can serve as a reference for evaluating regional and seasonal biases of current and future column CO₂ retrievals from both ground and satellite platforms.

2 Methods

2.1 Aircraft and tall tower sampling

Aircraft sampling in the NOAA GGRN intends to provide vertical profiles of long-lived trace gases to capture their seasonal and interannual variability. The aircraft sampling system consists of 12 borosilicate glass flasks in each programmable flask package (PFP), a stainless-steel gas manifold system, and a data logger and control. These flasks (0.7 L each) are pressurized to obtain 2.2 L of sample air from each target altitude. Air samples are then shipped back to NOAA/ESRL for carefully calibrated and quality-controlled measurements. Carbon dioxide is measured using a nondispersive infrared analyzer. Long-term measurements at ~ 15 sites are carried out using light aircraft that can reach 8.5 km. Air samples are collected mostly during late morning to early afternoon, when the air mass within the planetary boundary layer (PBL) is generally well mixed, and CO₂ enhancement near the ground from plant respiration during the night has been mixed throughout the boundary layer. Normally, the aircraft follows a pre-decided route such that most samples are collected within 0.1° of the site location. The sampling frequency varies from site to site, currently from twice a month to once every 1.5 months. For more sampling details, quality-control discussions, and an evaluation of the sampling frequency, please refer to Sweeney et al. (2015). More information on the aircraft sites can be found at <http://www.esrl.noaa.gov/gmd/ccgg/aircraft/>. We estimate the uncertainty of individual measurements of CO₂ in flask air (68 % confidence level) at 0.08 ppm. However, we have seen evidence of positive biases for samples collected using older flasks that may contain contaminants. Andrews et al. (2014) reported biases that increased from < 0.1 ppm in 2008 to an average offset in 2013 of 0.36 ppm. The aircraft sampling protocol was modified starting in August 2014 to mitigate this bias. For samples collected prior the protocol change, laboratory tests showed that new/clean flasks have zero bias, but some older/dirty flasks could have biases of > 1 ppm. This bias is not consistent among individual flasks and increases over time (Andrews et al., 2014); the potential bias is hard to quantify for measurements before August 2014. Thus, the high bias is not corrected in our study. More recently, low bias has been found in PFP measurements when the ambient humidity is high, based on comparisons of PFP measurements with data from in situ analyzers at tall towers. We are working to understand and quantify this bias, and for this study we have derived a preliminary correction factor, which shows a linear trend with -1.4 ppm CO₂ offset per 1 % above 1.7 % of ambient water (mole fraction relative to whole air) content. Only ~ 4 % of total aircraft measurements or ~ 12 % of those below 2 km are impacted by humidity higher than 1.7 %, for which we have applied corrections before data analysis. The mean correction applied is 0.53 ± 0.4 (1σ) ppm for the impacted data.

The NOAA tall tower network measures CO₂ and other trace gases within the continental boundary layer. Continuous in situ measurements are conducted using nondispersive infrared (NDIR) absorption sensors and cavity ring-down analyzers. The long-term stability of these systems is typically better than 0.1 ppm for CO₂ (Andrews et al., 2014). Most tall tower sites have more than one air intake height. In this study, continuous in situ measurements from the highest intake are used to minimize potential influences from local sources. More information concerning the tower sites can be found at <http://www.esrl.noaa.gov/gmd/ccgg/insitu/>. For the column XCO₂ calculation, tower data only from 10:00 to 17:00 local standard time (LST) on flight days are averaged to one data point per day, as a complement to vertical profiles within the PBL.

2.2 Site description

We analyze data from 19 aircraft sites and 6 tall tower sites during 2004 to 2014 (see Table S1 in the Supplement for a summary of site conditions). After considering the geographic distribution of these sites in North America, we group them into eight regions for spatial comparisons (Fig. 1). The northern west (NW) and southern west (SW) regions represent the inflow area on the west coast of the US, directly downwind of the Pacific Ocean at both higher elevations. The northern mid-continent (NM) region represents the boreal forest and agriculture region in north-central North America. The mid-continent (MC) region represents a dry landscape due to its high elevation (above 1.5 km on average) and semi-arid climate. The midwest (MW) region is strongly influenced by agriculture and temperate forest. The southern mid-continent (SM) represents the south-central humid temperate region, with inflow from the Gulf of Mexico during summer. The northeast (NE) region represents the temperate forest on the northeast coast of the US, which is mostly downwind of regions to the west above the PBL, and downwind of its southwest regions within the PBL. The southeast (SE) region represents the warm temperate region on the southeast coast of the US.

2.3 Smoothing of the reference data and column XCO₂ calculation

We use the Mauna Loa Observatory (MLO) as a reference site. MLO is located at 19.536° N, 155.576° W, and 3397 m above sea level. Carbon dioxide measurements from this site are widely used to represent background CO₂ in the Northern Hemisphere. For our study, a function consisting of a quadratic polynomial and four harmonics is fitted to the MLO data, adopted from the method described by Thoning et al. (1989). Residuals of the data from this function are smoothed by a low-pass filter with full-width at half-maximum in the time domain of 1.1 years. The smoothed residuals are then added back to the polynomial part of the

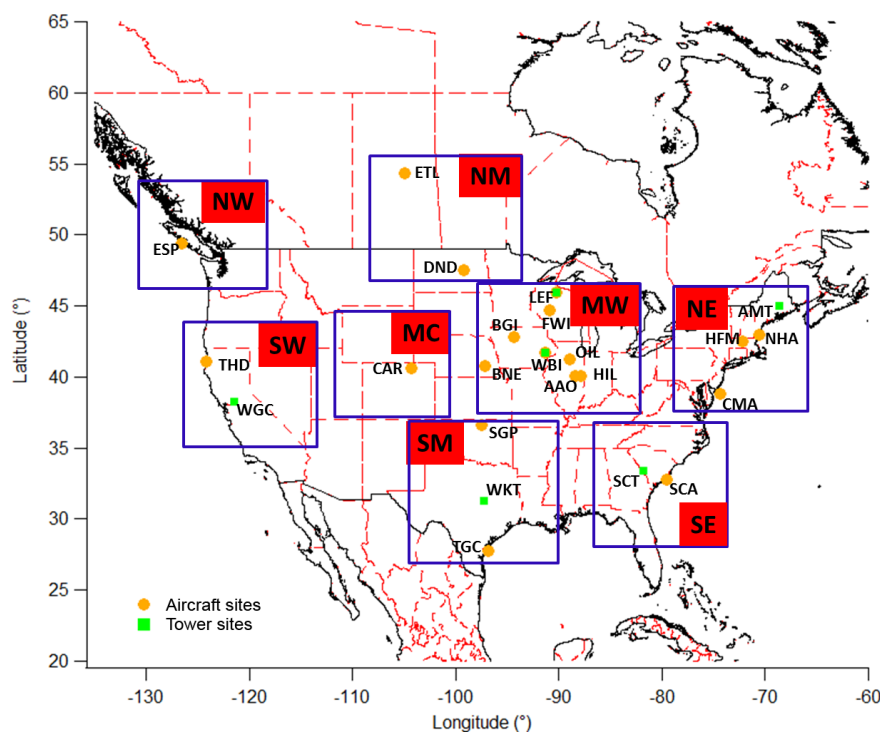


Figure 1. Aircraft, tall tower, and high-elevation/tower sites in the NOAA GGGRN. The eight boxes define regions that are further discussed for spatial pattern comparison. See Table S1 for detailed site information.

function to produce the long-term deseasonalized trend. This trend (see Fig. 3) is subtracted from all aircraft and tall tower measurements. Also, the CarbonTracker results presented in this study are the differences relative to observed MLO deseasonalized trend. We use “ Δ ” to represent detrended data in the following text and figures. The choice of reference site is not important for this study, since we focus on examining the relative seasonal patterns of the detrended spatial and vertical distributions of CO₂ instead of the total changes in CO₂ abundance attributed to global surface fluxes.

We calculate partial column average CO₂ dry mole fraction using tall tower and aircraft data, and the total column by adding simulations of high altitude CO₂ (above 330 hPa, ~ 8 km above sea level) from CarbonTracker. Since geometric height is available with each aircraft measurement, either from the onboard Global Positioning System (GPS) (after 2006) or inferred from the aircraft altimeter or pressure altitude, we first convert geometric height (in meters) to pressure (in hPa) for the pressure-weighted column XCO₂ calculation. This conversion uses geopotential data from NOAA/NCEP North American Regional Reanalysis (NARR) (Mesinger et al., 2006), available at <https://www.esrl.noaa.gov/psd/data/gridded/data.narr.html>, in which the geopotential is a function of latitude, longitude, pressure altitude, and time. We interpolate the geopotential field vertically to retrieve pressure and then calculate dry pressure by incorporating specific humidity data from NARR. Eventually, we use a trapezoidal

method to integrate over detrended vertical profiles for dry-pressure-weighted column averages. For the long-term averaged column Δ XCO₂ calculation, a long-term mean vertical profile is first constructed for each month by combining 11-year detrended data together and then averaging data in each 40 hPa vertical bin. To look at the long-term averaged total column Δ XCO₂ from individual aircraft sites, we combine aircraft data with upper-layer CT2015 simulations.

The NOAA CarbonTracker model assimilates CO₂ measurements from surface sampling networks and tall towers to generate global 3-D fields of atmospheric CO₂ mole fraction. The CarbonTracker model has evolved significantly since Peters et al. (2007). A detailed description of this model is provided in documents available at <http://carbontracker.noaa.gov>. Our study utilizes CarbonTracker results from the 2015 release (CT2015). This version provides CO₂ mole fraction over North America with $1^\circ \times 1^\circ$ spatial and 3 h temporal resolutions, which are analyzed in Sect. 3.2 and 3.3. Total column CO₂ calculated from CT2015 global data with $3^\circ \times 2^\circ$ spatial resolution is also presented in the Supplement. We have evaluated the performance of CarbonTracker in the upper atmosphere (330 to 0 hPa) by comparing its simulations with in situ measurements from nine AirCore profiles (Karion et al., 2010) sampled in 2012–2014. AirCore is a ~ 150 m stainless-steel tube that utilizes changes in ambient pressure for passive sampling of the vertical profile. The tube is carried to high altitude by a balloon and it collects

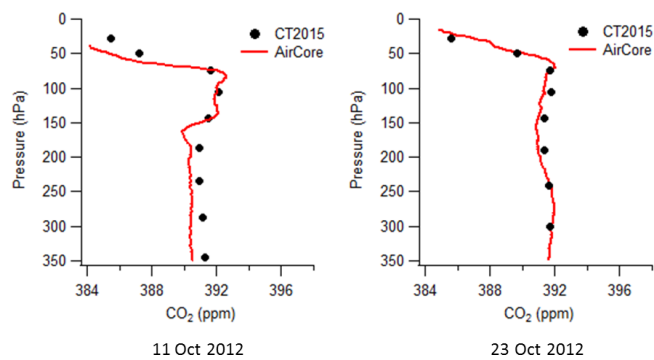


Figure 2. CarbonTracker (CT2015) simulations compared with AirCore in situ measurements in the upper atmosphere. AirCore profiles in the left and right panels are sampled near CAR and SGP, respectively.

a continuous sample as it descends. It is then measured by an analyzer after it is recovered. More information about the AirCore system can also be found at <https://www.esrl.noaa.gov/gmd/ccgg/aircore/>. All nine AirCore profiles are taken near Southern Great Plains, Oklahoma (SGP) and Briggsdale, Colorado (CAR) (see Fig. 1 for site locations.) Figure 2 shows examples of AirCore profiles compared with CT2015 in the upper atmosphere, which demonstrates good agreement. We also compare partial column (330 to 0 hPa) averages from the nine AirCore profiles and CT2015. Results from CT2015 agree generally well with AirCore, with differences ranging from 0.03 to 1.22 ppm (mean value equals 0.66 ppm), which suggests that CT2015 may have a high bias that could contribute to $0.66 \times 1/3 = 0.22$ ppm overestimation on average to the total column average. However, AirCore is in the process of rigorous evaluation; the differences between AirCore and CT2015 are not well characterized yet, since we only have a limited amount of AirCore data. It is unclear whether the potential bias of CT2015 in this partial column is dependent on time or sampling location. Adding a constant bias correction to all regions will not change the spatial gradients that we focus on in this study. Thus, no correction is applied when using CT2015 simulations to represent the upper third of the total column. For uncertainty estimates, we use a “bootstrap” method that uses random resampling of individual vertical profiles with restitution (low bias, high humidity was corrected), with 100 Monte Carlo runs for each column average calculation. Uncertainty is then defined as 1 standard deviation of the 100 Monte Carlo results.

3 Results and discussions

3.1 Seasonal patterns and spatial gradients

Typically, one aircraft profile contains measurements at 12 different altitudes. Column ΔXCO_2 can be computed for each profile using the method described in Sect. 2.3 (Fig. S1

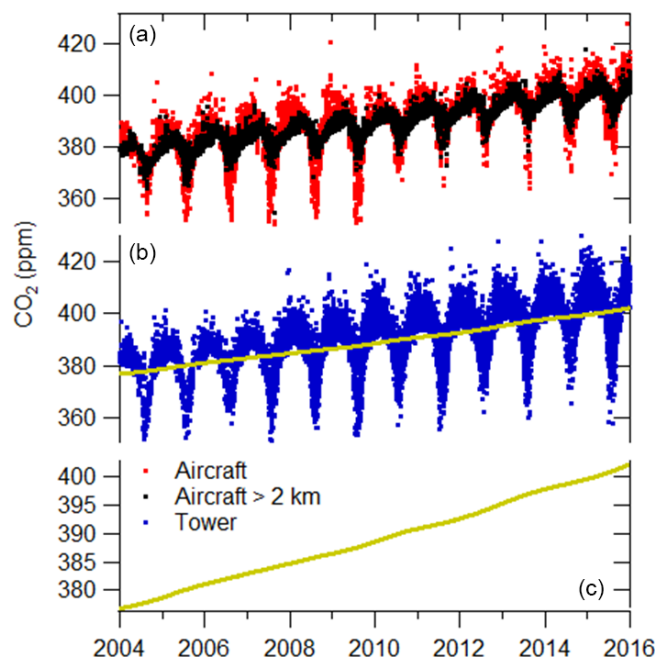


Figure 3. CO₂ observations from aircraft (a) and towers (b). The yellow line in panel (b) illustrates the deseasonalized trend at the Mauna Loa Observatory (MLO), the same as in (c), in which the y axis is expanded.

in the Supplement). Our aircraft- and CT2015-based column CO₂ at the SGP and LEF (see Fig. 1 for site locations) sites shows reasonable agreements with TCCON data retrieved at the Lamont and Park Falls sites (Washenfeller et al., 2006; Wunch et al., 2009, 2011), respectively (Fig. S2). Figure 3 shows aircraft (at all altitudes) and tower data (daily averages for 10:00–17:00 LST data) from all sites used in this study. Aircraft data above 2 km exhibit much smaller seasonal variations than the full dataset, because the variations are mainly driven by CO₂ sources and sinks near the Earth’s surface. CO₂ mole fraction is enhanced in the shallow wintertime PBL primarily due to reduced plant photosynthesis and ecosystem respiration combined with slightly increased fossil fuel emissions. During summer, the PBL is deeper, and depletions within the PBL are due to strong terrestrial uptake that dominates over emissions especially from June to August. During the summers of 2010 to 2012, CO₂ from aircraft measurements appears higher than in other years in Fig. 3; however, similar characteristics are not present in tower data. This apparent difference is due to a decrease in sampling frequency at several aircraft sites that resulted in an aliased picture of the full summer signals. Since we focus on the climatological mean of 11 years of data in our study, this influence is eliminated by combining 11 years of data together into one “average year”.

To investigate the contributions of different altitudes to spatial gradients between regions, we divided all measurement data into three layers according to their sampling alti-

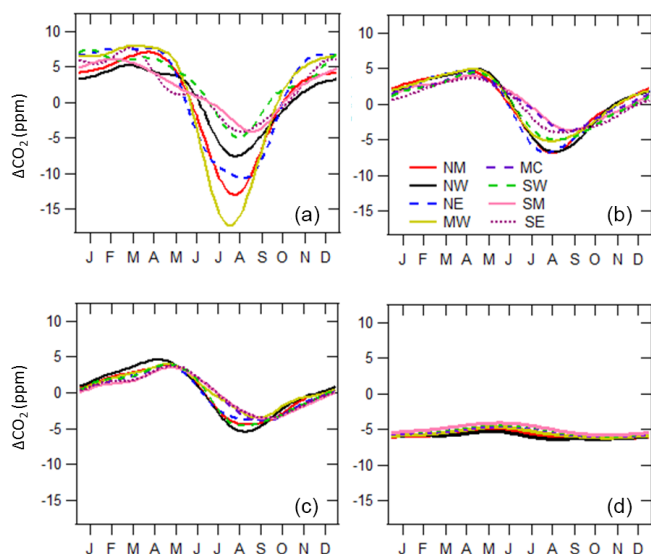


Figure 4. Multi-year (2004–2014) average smooth seasonal curves of CO₂ relative to the long-term deseasonalized trend at Mauna Loa for different vertical layers: (a) aircraft and tower data under 2 km – MC is not presented because only limited data were available due to high surface elevations (> 1.5 km on average) in this region; (b) aircraft data from 2 to 5 km; (c) aircraft data from 5 to 8.5 km; (d) CT2015 model results for layers above 330 hPa (~8.5 km) to 0 hPa (~80 km).

tudes: below 2, 2–5, and 5–8.5 km m a.s.l. (Fig. 4). Smooth seasonal curves are attained from fitting data with four harmonics using the method described by Thoning et al. (1989). The peak-to-valley amplitudes of the seasonal cycles below 2 km are the largest among the three layers for most regions, with a minimum of 10.3 ppm in SM and a maximum of 25.0 ppm in MW. The seasonal variation amplitudes decrease to 7.7–11.5 ppm in the 2–5 km layer and further decrease to 7.2–10.0 ppm in the 5–8.5 km layer. We also observe that the seasonal cycle drawdown occurs later in the layers above 2 km (see Fig. S3, which provides similar information as Fig. 4, but seasonal curves from different vertical layers are grouped by regions to facilitate comparisons of the phases of seasonal cycles). The seasonal CO₂ drawdown below 2 km is mainly influenced by terrestrial photosynthesis, and gradients are due to local to regional fluxes, with an earlier onset of drawdown in southern regions than in northern regions. The seasonal cycle aloft is damped and lagged compared to the PBL, with influences from throughout the Northern Hemisphere and with spatial gradients likely driven by large-scale transport. The NW, SW, SM, and SE inflow regions have significant delays of more than 1 month in the 2–5 km layer compared with the surface layer, which is likely due to the delayed phase of the seasonal cycle in well-mixed air coming from the oceans. Vertical homogeneity of air over ocean was observed during the HIAPER Pole-to-Pole Observations (HIPPO) aircraft campaign (Wofsy et al., 2011;

Frankenberg et al., 2016). As air masses are transported further inland, we observe reduced discrepancies of the timing of CO₂ drawdown between surface and upper-layer air (2–5 km), which may be associated with the increased influence of the land surface in the mid-troposphere due to strong convection over land. CO₂ drawdown in the 5–8.5 km layers also occurs later than in the 2–5 km layers in most regions; however, differences between these two layers are small. The declining amplitude and delayed phase of the seasonal cycle with altitude have been noted often (e.g., Tanaka et al., 1983; Ramonet et al., 2002; Gerbig et al., 2003; Sweeney et al., 2015). It demonstrates that there is a lot of important information in the vertical profile that is diminished in observations of the total column.

We find that the largest horizontal spatial gradients between regions occur below 2 km during summertime (Fig. 4), with a maximum difference of ~15.5 ppm between MW and SM. SM and SW exhibit less-pronounced seasonal cycles, which is likely associated with air masses from the Gulf of Mexico and the Pacific Ocean, respectively, whereas MW exhibits a deep summer drawdown (amplitude in seasonal cycles) partially as a result of strong regional forest and crop uptake. Crevoisier et al. (2010) estimated the surface flux over North America using vertical CO₂ measurements and average wind vectors, and reported that annually averaged land carbon fluxes in the western (including SW) and southern regions (including SM) were neutral. The SE region also demonstrates a less pronounced seasonal cycle with higher summertime levels compared with other northern regions, which may be due to the sea-breeze influence in summer within the PBL. In wintertime, CO₂ levels in NE and MW are higher than in other regions, which result from regional fossil fuel and terrestrial biogenic emissions combined with transport from the west and south.

Higher-altitude data (above 2 km) exhibit only small spatial gradients. In the 2–5 km layer, the largest gradient is 4 ppm in summer (Fig. 4b). It further decreases to less than 3 ppm in the 5–8.5 km layer (Fig. 4c). Figure 4d shows modeled CO₂ mole fractions from CT2015 for the upper troposphere and above (330 to 0 hPa), which are used to fill in above the aircraft profiles for calculation of total column ΔX_{CO_2} . Spatial gradients in this layer are less than 0.5 ppm, suggesting that the top third of the total column has little contribution to the spatial gradients of the total column.

3.2 Long-term mean vertical profiles

To investigate the mean spatial gradients, we first calculate the long-term mean monthly vertical profiles as described in Sect. 2.3. In addition, each tower serves as one additional layer in the mean profile. The long-term mean tower data generally fit well in the vertical profiles from measurements of aircraft samples (Figs. 5 and 6), suggesting that the biases described in Sect. 2.1 do not significantly affect the long-term mean. To attain profiles of the entire atmospheric col-

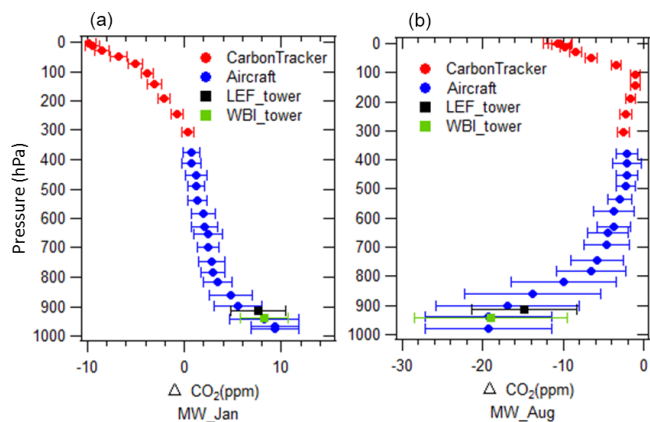


Figure 5. Long-term mean (2004–2014) average vertical profiles in January (a) and August (b) in MW. The error bar shows 1 standard deviation.

umn, upper layers (330 to 0 hPa) are filled in by CT2015, and the lowest data point of the measured profile is extended to ground level, defined by the mean surface elevation in that region.

Figure 5 presents two examples of long-term mean profiles with data variability, which is 1 standard deviation for each 40 hPa bin of aircraft data or for all flight-day tower data. Variability as large as 20 ppm is seen within the PBL in the MW region in summer, which is due to strong and heterogeneous surface vegetation uptake and ecosystem respiration combined with day-to-day changes in wind direction. All long-term mean monthly vertical profiles are presented in Fig. 6, which shows the mean temporal and vertical variability of CO₂ in each season and further demonstrates the vertical propagation of seasonal CO₂ due to changes of surface flux. In wintertime, monotonic decrease of CO₂ with altitude can be observed from all regions, in which high PBL CO₂ is mainly driven by surface emissions and reduced vertical mixing (Denning et al., 1999; Stephens et al., 2007). Surface CO₂ decreases dramatically in the growing season in those regions influenced by high plant activity, such as the NM and MW regions. For the summer vertical profiles in the NE and SE regions (east coast of the US), the CO₂ mixing ratio is elevated in the layer under 900 hPa, followed by significant decreases in the upper layers until 750 hPa, and then increases with altitude until tropopause (Fig. 6). This is likely a result of sea breeze influence. Lower-troposphere air from the sea, lacking terrestrial uptake of CO₂, typically has higher CO₂ in summer compared with inland air. Polluted air previously advected offshore can be brought back along with sea breeze. Without significant vertical mixing over the marine surface, high levels of pollutants remain in those air masses. The convergence of sea breeze with prevailing wind moving offshore may create a period with a stalled frontal structure that can aggregate air pollutants (Banta et al., 2005). The convective internal boundary layer structure of the sea breeze system

can significantly reduce mixing height (Miller et al., 2003), and also induces higher CO₂ levels. When the sea breeze is not dominant, air advected from the southwest and west (the land) can also bring in polluted air with high CO₂ since this region is downwind of continental US emissions (Miller et al., 2012).

3.3 Partial column ΔXCO₂ and total column ΔXCO₂

Seasonal variations of monthly averaged partial column ΔXCO₂ (below 330 hPa) demonstrate maximum values in April and minimum values in August or September (Fig. 7a). The largest amplitude appears in NM, with peak-to-valley difference up to 13.5 ppm. SW, SM, SE, and MC have similar amplitudes of 7–8 ppm, smaller than the other three regions. To evaluate the performance of CT2015 on column ΔXCO₂, CT2015 results are sampled to match the latitude, longitude, altitude, and time of actual measurements (CarbonTracker Team, 2016). Note that aircraft profiles are not assimilated in CT2015, so aircraft data are independent of the CT2015 data assimilation. Figure 7b shows monthly partial columns of ΔXCO₂ calculated from CT2015, which demonstrate good agreement with results from measurements. Only small seasonal biases exist in CT2015, with high bias occurring mostly in spring and early summer and low bias in September and October (Fig. S4). The overall differences of monthly partial column ΔXCO₂ (CT2015–measurements) mainly fall in the range of −0.64 ppm (5th percentile) to 0.84 ppm (95th percentile) with a mean difference of 0.13 ppm. These differences are of similar magnitude to the uncertainties of partial column ΔXCO₂ calculated from the measurements (Fig. S5). It is clear that CT2015 captures the long-term mean variations of both phase and amplitude of partial column XCO₂ reasonably well when compared with well-calibrated measurements across North America.

Total column ΔXCO₂ is presented in Fig. 7c. In NW, NM, NE, and MW, seasonal variations of total column ΔXCO₂ are very similar in both phase and amplitude (8–9 ppm peak to valley). For SW, SM, SE, and MC, amplitudes are ~5.5 ppm. The smallest spatial gradients occur during May and October, which result in maximum differences among all regions of only 0.9 and 0.7 ppm, respectively. The largest spatial gradients occur during June, July, and August, which result in maximum differences of 2.4, 4.5, and 4.1 ppm, respectively. It is interesting that the deepest seasonal draw-down is seen in NM, not in MW that encompasses the very intensive agricultural activities in the US midwest, which suggests the possibility of strong upwind influence in the NM region. Transported signals have significant influences on total column CO₂. The summer total column ΔXCO₂, represented by the June–August average from CT2015, has a magnitude that is similar to observations with differences of no more than 1 ppm (Fig. 8). Based on the seasonal patterns of total column ΔXCO₂ (Fig. 7c) and the summer column ΔXCO₂ (Fig. 8), we can separate the eight regions into two

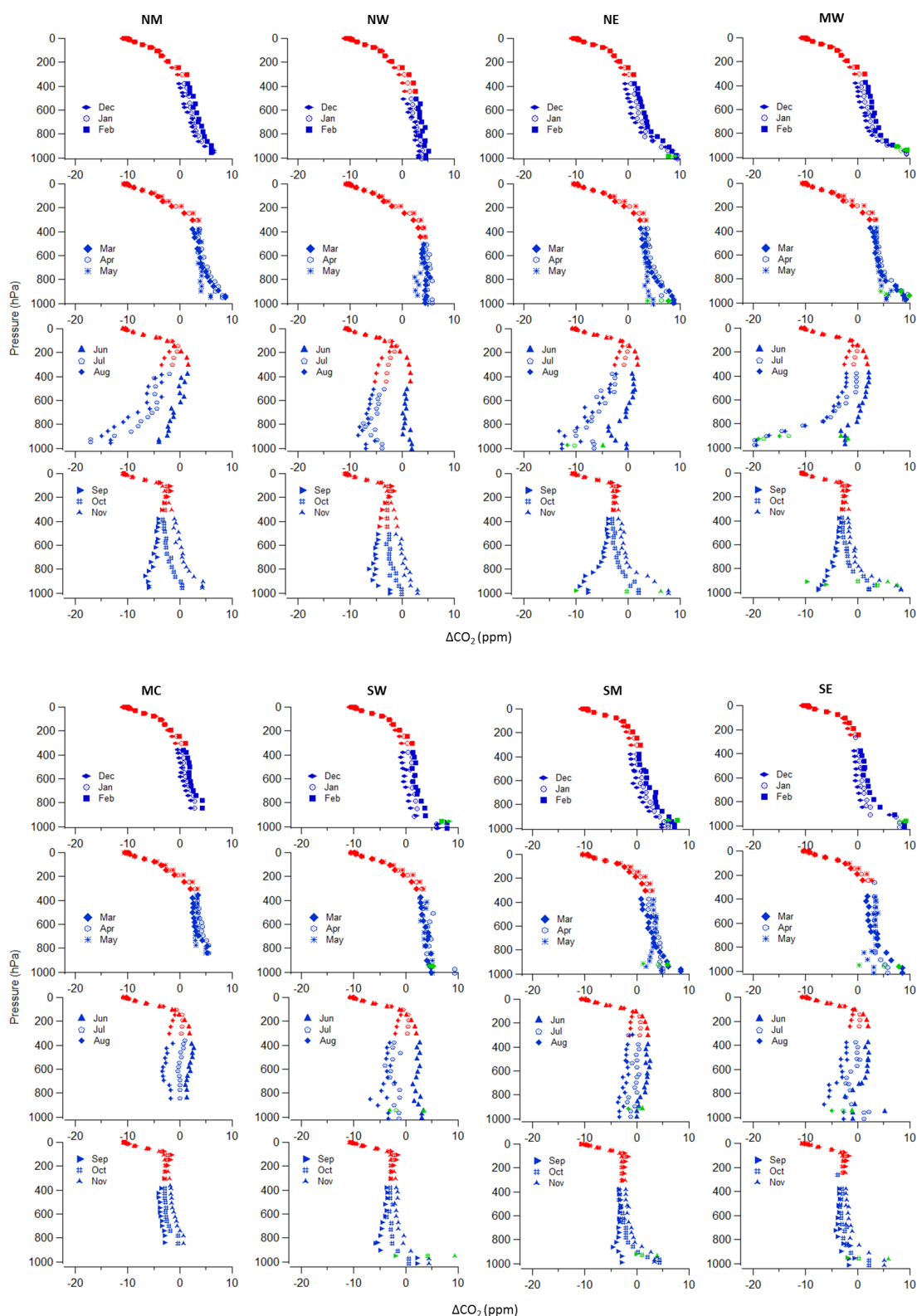


Figure 6. Long-term mean (2004–2014) monthly vertical profiles in NM, NW, NE, MW (by column, from left to right in the upper panel) and in MC, SW, SM, SE (by column, from left to right in the bottom panel). Blue points were calculated from observations, red points were calculated from CT2015, and green points were calculated from tower data.

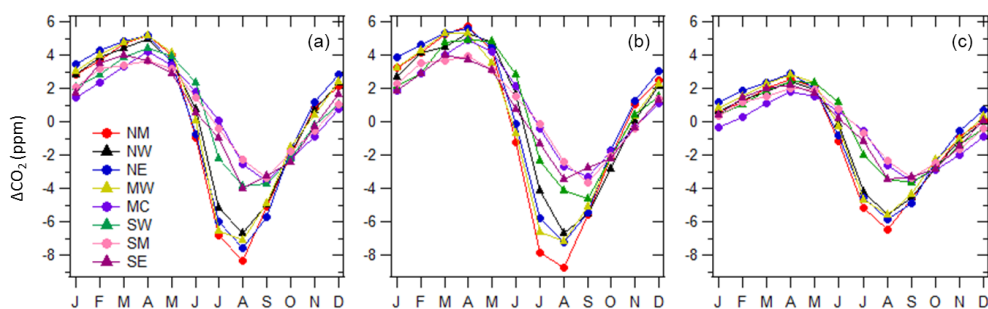


Figure 7. (a) Partial column ΔXCO_2 calculated from aircraft and tower data; (b) partial column ΔXCO_2 calculated from CT2015; (c) total column ΔXCO_2 calculated from aircraft and tower data, including the top-layer data from CT2015.

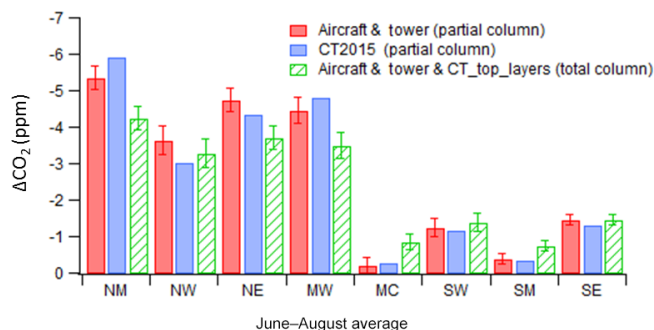


Figure 8. Long-term mean (2004–2014) for June–August partial and total column ΔXCO_2 . The error bars represent 1 standard deviation from the bootstrap uncertainty calculation (see Sect. 2.3).

groups. The group with NW, NM, NE, and MW has ~ 3 ppm stronger drawdown (larger amplitude) than the group with SW, SM, SE, and MC. For winter total column ΔXCO_2 (December to February average), the maximum spatial difference is only 1.6 ppm, with the highest total column ΔXCO_2 of 1.2 ppm in NE and the lowest value of -0.3 ppm in MC.

3.4 Influence of large-scale circulation

Figure 9 shows long-term mean summer column ΔXCO_2 calculated from CT2015, together with full column ΔXCO_2 from individual aircraft sites. Note that some aircraft sites have less than 11 years of data that CT2015 shows in Fig. 9, and only aircraft sites with more than 6 years of data are presented; the actual values are provided in Table S2. The fact that total column ΔXCO_2 from CT2015 agrees well with aircraft sites supports the performance of CT2015 on a long-term average basis. The observations show a similar summer spatial pattern, with lower column ΔXCO_2 in the north and northeast regions and higher column ΔXCO_2 in the south and southwest regions (Fig. 9a). Scattered hot spots of high column ΔXCO_2 associated with surface emissions from megacities, or cold spots associated with strong local uptake, are not or just barely visible in the long-term average column ΔXCO_2 map at $1^\circ \times 1^\circ$ resolution. Instead,

the wave-like pattern of column ΔXCO_2 over North America reflects the average large-scale circulation. To support our hypothesis on the influence of large-scale circulation, we analyze the long-term mean wind pattern over North America. We can see that air masses from northwest of the continent bring in low average column ΔXCO_2 , while air masses from the south (mainly the subtropical Pacific Ocean and the Gulf of Mexico) bring in high column ΔXCO_2 (Fig. 9b). The zonal gradients over the continent, especially north of $40^\circ N$, also reflect long-term average wind patterns; southwest wind corresponds to higher column ΔXCO_2 over the western part of the continent until the wind direction shifts to west–northwest over the eastern part of the continent. This wind pattern matches well with the geographic division of the over/under -3 ppm areas colored in green/blue in the column ΔXCO_2 map (Fig. 9b). Figure 9c and d shows partial column averages for the free troposphere (800–330 hPa) and lower troposphere (below 800 hPa), respectively. The free troposphere spatial gradient also demonstrates a wave-like pattern. A previous study on the total column CO₂ from the ground-based TCCON found strong correlation between the midlatitude column CO₂ and synoptic-scale variation of potential temperature (θ , at 700 hPa), a dynamic tracer for adiabatic air transport (Keppel-Aleks et al., 2012). Thus, they also propose that the variations in column CO₂ are mainly driven by large-scale flux and transport. Analysis of the interannual variability of the seasonal cycle amplitudes of column CO₂ in the Northern Hemisphere has also found a significant contribution of large-scale circulations to the north–south gradient (Wunch et al., 2013).

The strong drawdown over northeast North America in summer is a consequence of long-range transport of low CO₂ from northeast Eurasia, in addition to regional terrestrial uptake. Sweeney et al. (2015) notes well-mixed vertical profiles (up to 8 km) of CO₂, CO, CH₄, N₂O, and SF₆ from the THD (Trinidad Head, California), ESP (Estevan Point, BC, Canada), and PFA (Poker Flat, Alaska; $65.07^\circ, -147.29^\circ$) sites and suggests that air coming across the Pacific was strongly influenced by Asian surface fluxes before being vertically homogenized as it passed over the Pacific

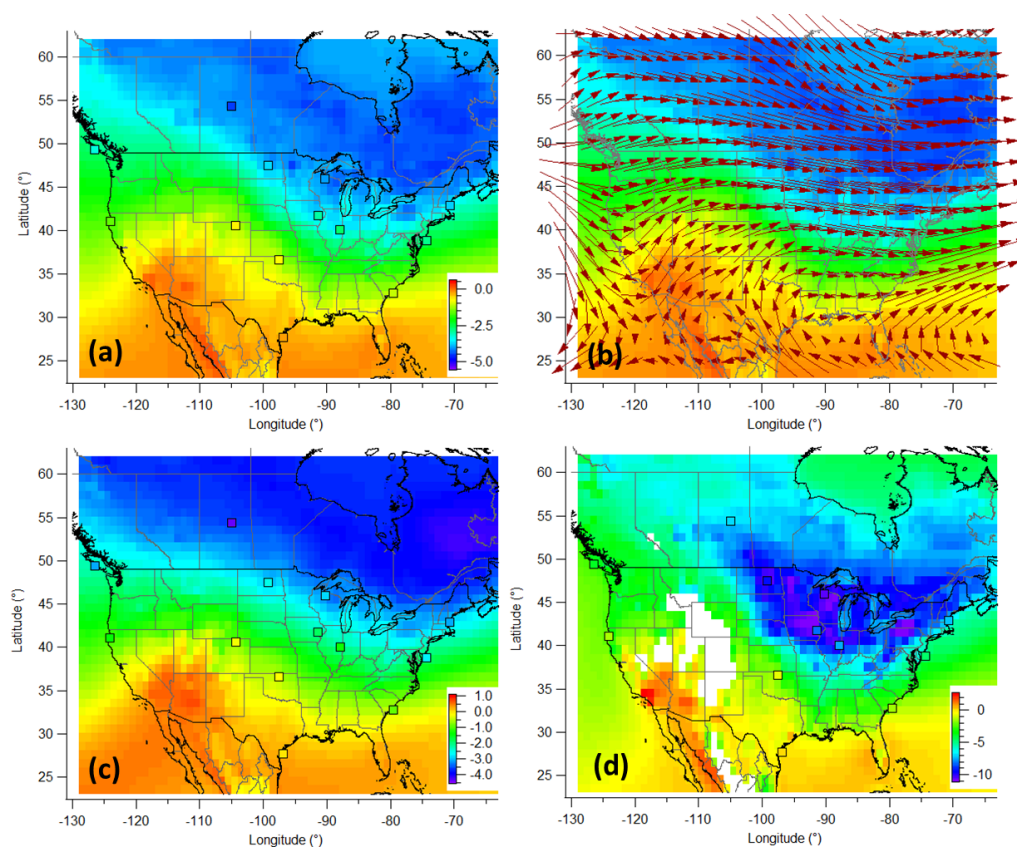


Figure 9. Long-term mean (2004–2014) for June–August total column ΔXCO_2 (in ppm) from CT2015 in $1^\circ \times 1^\circ$ spatial resolution with total column ΔXCO_2 for 13 individual aircraft sites in squares (a), and CT2015 column ΔXCO_2 overlaid with pressure-weighted (1000 to 500 hPa) mean wind vectors for the same period (b). Panels (c) and (d) are similar to (a), except for the free troposphere (800 to 330 hPa) and lower troposphere (below 800 hPa), respectively. Note the different color scales.

Ocean. This well-mixed air forms an important boundary condition in the column CO₂ of air coming into the North American continent. This was best illustrated at sites like PFA where the summertime minimum in CO₂ significantly preceded maximum ecosystem uptake of CO₂, implying significant influence of transported air from lower-latitude regions from Asia. We further conduct an experiment using CarbonTracker to investigate the importance of this effect. A control run and a “masked run” are conducted for 2010–2012, in which the Eurasian boreal flux is turned on/off. The MLO CO₂ trend from each model scenario is used as reference background and thus removed before total column ΔXCO_2 calculation. Figure 10 shows the results for summer 2012, which is an average summer when compared with the 2004–2014 mean pattern (Figs. 9 and 11). The maximum north–south difference reduces to ~ 2.5 ppm after we turn off the Eurasian boreal flux, compared with ~ 5 ppm from the control run. In both the control and masked scenarios, the free troposphere partial ΔXCO_2 demonstrates similar spatial patterns to total column ΔXCO_2 (Fig. S6). This result combined with results from Sweeney et al. (2015) demonstrates that the transport of low CO₂ resulting from large summer-

time Eurasian boreal uptake has a large contribution on the overall summer total column CO₂ decrease in North America.

3.5 A comparison with apparent gradients over Europe

Figure 11 shows the climatological June–August mean modeled global column ΔXCO_2 map in $3^\circ \times 2^\circ$ spatial resolution, which presents smooth wave-like patterns. Reuter et al. (2014) use SCIAMACHY and GOSAT satellite retrievals of column CO₂ and inverse modeling to infer a very large net CO₂ uptake flux over the European region. Column ΔXCO_2 from CT2015 (Fig. 11) exhibits a drastically different summer spatial pattern over Europe compared with the 8-year mean (2003–2010) June through August satellite retrievals presented by Reuter et al. (2014, their Fig. 2a). The spatial gradient from CT2015 results in a maximum 3–4 ppm difference and a gradual pattern, instead of as much as 6 ppm from satellite retrievals. There is no sign of XCO₂ hot spots from surface emissions or removals in the CT2015 spatial pattern over Europe (Fig. 11), in contrast to several hot spots that are apparent from the 8-year averaged SCIAMACHY satellite

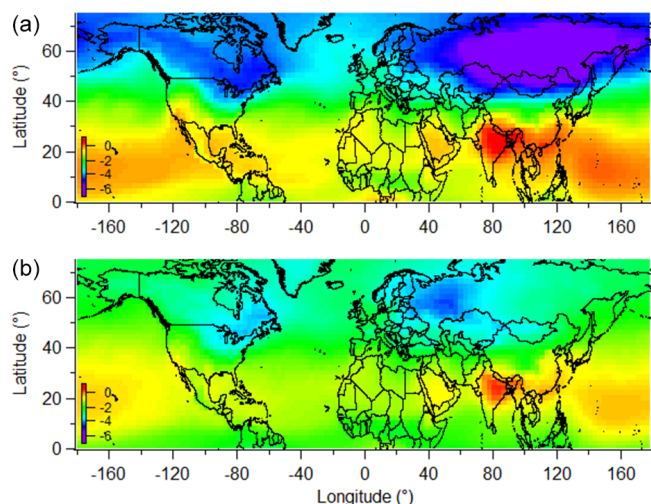


Figure 10. Total column ΔXCO_2 (in ppm) from the CarbonTracker control (a) and masked (b, Eurasian boreal flux is masked) runs for June–August 2012 ($3^\circ \times 2^\circ$ spatial resolution). MLO trend from each individual scenario is removed before the ΔXCO_2 calculation. The same color scale is used as in Fig. 9a. Partial column ΔXCO_2 patterns for the free troposphere (800 to 330 hPa) and lower troposphere (below 800 hPa) are provided in the Supplement.

retrievals over Ireland, the UK, Belgium, the Netherlands, north of Germany, and south of Sweden, and low spots over Ukraine and Kazakhstan (Reuter et al., 2014). This SCIAMACHY retrieval pattern contradicts our understanding of the significant influence of large-scale transport on column ΔXCO_2 . Although the NOAA/ESRL CT2015 (<https://www.esrl.noaa.gov/gmd/ccgg/carbontracker/CT2015/>) assimilates fewer observations over Europe than CarbonTracker Europe (<http://www.carbontracker.eu/>), both models produced similar fluxes over the European region (see both websites for detailed fluxes). The $3^\circ \times 2^\circ$ grid from CT2015 is not likely responsible for a much smoother pattern for CarbonTracker, compared with the $2^\circ \times 2^\circ$ grid from satellite retrievals (Reuter et al., 2014). The North American region on the $3^\circ \times 2^\circ$ grid in Fig. 11 shows a similar pattern to the $1^\circ \times 1^\circ$ grid in Fig. 9, with similar spatial difference of ~ 5 ppm. A smoother spatial distribution should be expected in Europe for the long-term mean column XCO_2 (Fig. 11) due to the influences of dominating west and southwest winds in summer. We have also evaluated the importance of sampling bias by sampling CT2015 at the same latitude/longitude/hour (within 1 h) as in SCIAMACHY Bremen optimal estimation (BESD v02.00.08) data (Reuter et al., 2011). The 8-year mean pattern shows much smaller gradients (3–4 ppm maximum) without significant hot/cold spots at the locations of SCIAMACHY (Fig. S7). Although sampling biases contribute to the unphysical column XCO_2 spatial pattern from SCIAMACHY, they cannot explain the large gradients. When we compare CT2015 directly with SCIAMACHY BESD data, we find up to ~ 3 ppm differences over

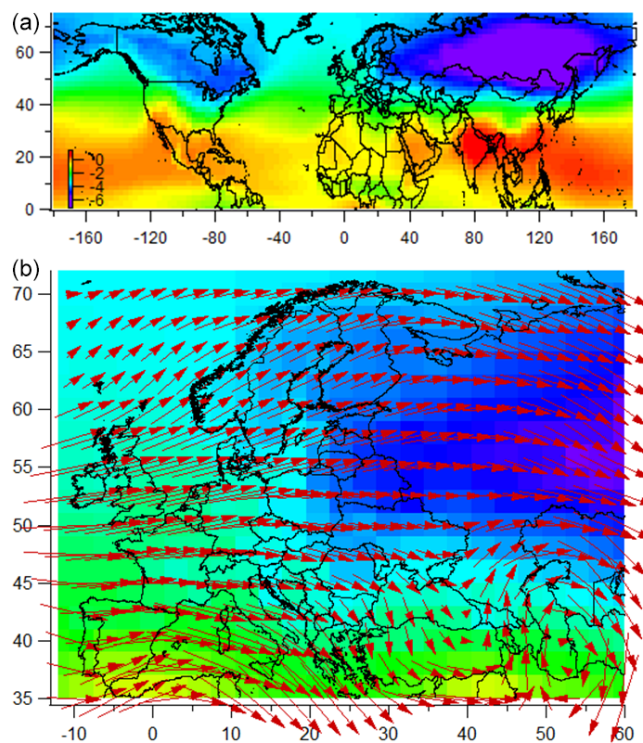


Figure 11. Long-term mean (2004–2014) for June–August total column ΔXCO_2 (in ppm) from CT2015 (a) in $3^\circ \times 2^\circ$ spatial resolution, and detail for Europe overlaid with pressure-weighted (1000 to 500 hPa) mean wind vectors for the same period (b). The color scale is the same as in Fig. 9a, which is scaled to reflect 6 ppm difference of XCO_2 to compare with satellite retrievals from Reuter et al. (2014, their Fig. 2a).

North America and Europe (Fig. S8). Since CT2015 compares well with calibrated data over North America, we are deeply skeptical about any sources/sinks inferred from the SCIAMACHY BESD data. A recent study (Feng et al., 2016) using inverse modeling suggests that satellite retrievals outside the immediate European region and a small bias of only 0.5 ppm were sufficient to produce the apparent large carbon sink in the study of Reuter et al. (2014). This is expected from elementary mass balance considerations as in Sect. 1. Spatial gradients are the fundamental signals to infer regional fluxes. Since spatial gradients from CT2015 are realistic, boreal fluxes inferred by CT2015 should be more trustworthy than fluxes estimated based on unrealistic spatial patterns. The European carbon sink is still inconclusive; the discrepancies among different methods and results are further discussed by Reuter et al. (2017).

4 Conclusions

Aircraft and tall tower measurements from the NOAA GGGRN provide detailed information describing the long-term average temporal and spatial variations of CO₂ in the

PBL and the free troposphere. These data provide valuable constraints for evaluating model simulations and satellite retrievals. Seasonal cycle peak-to-peak amplitudes of CO₂ are largest below 2 km, where those maximum values are about twice those in the vertical layers above, indicating that most of the information on surface sources and sinks resides in the continental PBL. Large spatial gradients of CO₂ over North America are observed below 2 km during summer (with a maximum difference of ~ 15.5 ppm between MW and SM), while higher-altitude data (above 2 km) have much smaller contributions to spatial gradients, with a maximum difference of 4 ppm. The spatial differences of CO₂ in the upper troposphere and above (330 to 0 hPa) are less than 0.5 ppm, according to CT2015. Comparison with AirCore measurements shows CT2015 performs well at simulating upper tropospheric and lower stratospheric patterns.

Our long-term mean vertical profiles show that tower data agree well with aircraft data at similar vertical levels. Partial column ΔXCO_2 was calculated from the long-term mean vertical profiles. By comparing the partial column ΔXCO_2 from measurements with those from CT2015, we verify that CT2015 captures the long-term mean patterns of both phase and amplitude of partial ΔXCO_2 .

Large spatial gradients of ΔXCO_2 only appeared in summer, during which time the north and northeast regions had ~ 3 ppm stronger drawdowns than the south and southwest regions. Scattered hot spots of high column ΔXCO_2 associated with surface emissions from megacities, or cold spots associated with strong local uptake, are not or just barely visible in the long-term average column ΔXCO_2 . Instead, the wave-like pattern of column ΔXCO_2 over North America matches well with the average large-scale circulation. A CarbonTracker experiment to investigate the impact of Eurasian long-range transport suggests that the large summertime Eurasian boreal flux alone contributes about half of the north–south column ΔXCO_2 gradient across North America. Considering the transported signals from other upwind regions, including northern Canada, we expect that the transported signals have the overall largest contribution to the total column ΔXCO_2 spatial gradient.

Data availability. CarbonTracker CT2015 data are available at <https://www.esrl.noaa.gov/gmd/ccgg/carbontracker/CT2015/> (NOAA, 2015).

Measured CO₂ mole fractions from aircraft and tall towers, and CT2015 simulations of those measurements are publicly available from the data package `obspack_co2_1_CARBONTRACKER_CT2015_2016-03-12`, available at <https://doi.org/10.15138/G3H59M> (NOAA, 2016).

AirCore data are available at <https://doi.org/10.15138/G3N33W> (Sweeney et al., 2017).

The Supplement related to this article is available online at <https://doi.org/10.5194/acp-17-15151-2017-supplement>.

Author contributions. XL was responsible for study design, data analysis, and manuscript writing. PT was responsible for study design, data analysis, and manuscript improvement. CS and AA provided measurement data and improved the manuscript. AJ provided modeled data and improved the manuscript. ED analyzed measurements, ensured data quality, and improved the manuscript. JK conducted tower measurements and improved the manuscript. MC, PL, and SW analyzed measurements and ensured data quality. KT provided the data smoothing method.

Competing interests. The authors declare that they have no conflict of interest.

Acknowledgements. We especially thank Sourish Basu for helpful advice on satellite data, and John Mund for extracting NARR meteorological variables for our measurements. CarbonTracker CT2015 results are provided by NOAA ESRL, Boulder, Colorado, USA, from the website at <http://carbontracker.noaa.gov>. This research was supported by a fellowship from the National Research Council Research Associateship Programs.

Edited by: Christoph Gerbig

Reviewed by: three anonymous referees

References

- Andrews, A. E., Kofler, J. D., Trudeau, M. E., Williams, J. C., Neff, D. H., Masarie, K. A., Chao, D. Y., Kitzis, D. R., Novelli, P. C., Zhao, C. L., Dlugokencky, E. J., Lang, P. M., Crotwell, M. J., Fischer, M. L., Parker, M. J., Lee, J. T., Baumann, D. D., Desai, A. R., Stanier, C. O., De Wekker, S. F. J., Wolfe, D. E., Munger, J. W., and Tans, P. P.: CO₂, CO, and CH₄ measurements from tall towers in the NOAA Earth System Research Laboratory's Global Greenhouse Gas Reference Network: instrumentation, uncertainty analysis, and recommendations for future high-accuracy greenhouse gas monitoring efforts, *Atmos. Meas. Tech.*, 7, 647–687, <https://doi.org/10.5194/amt-7-647-2014>, 2014.
- Banta, R. M., Senff, C. J., Nielsen-Gammon, J., Darby, L. S., Ryerson, T. B., Alvarez, R. J., Sandberg, S. R., Williams, E. J., and Trainer, M.: A bad air day in Houston, *B. Am. Meteorol. Soc.*, 86, 657–669, <https://doi.org/10.1175/BAMS-86-5-657>, 2005.
- Biraud, S. C., Torn, M. S., Smith, J. R., Sweeney, C., Riley, W. J., and Tans, P. P.: A multi-year record of airborne CO₂ observations in the US Southern Great Plains, *Atmos. Meas. Tech.*, 6, 751–763, <https://doi.org/10.5194/amt-6-751-2013>, 2013.
- CarbonTracker Team: Simulated observations of atmospheric carbon dioxide from CarbonTracker release CT2015 (`obspack_co2_1_CARBONTRACKER_CT2015_2016-03-12`), including measured values from a multi-laboratory compilation of CO₂ observations, NOAA Earth System Research Laboratory,

- Global Monitoring Division, <https://doi.org/10.15138/G3H59M>, 2016.
- Chevallier, F., Palmer, P. I., Feng, L., Boesch, H., O'Dell, C. W., and Bousquet, P.: Towards robust and consistent regional CO₂ flux estimates from in situ and space-borne measurements of atmospheric CO₂, *Geophys. Res. Lett.*, 41, 1065–1070, <https://doi.org/10.1002/2013GL058772>, 2014.
- Choi, Y. H., Vay, S. A., Vadrevu, K. P., Soja, A. J., Woo, J. H., Nolf, S. R., Sachse, G. W., Diskin, G. S., Blake, D. R., Blake, N. J., Singh, H. B., Avery, M. A., Fried, A., Pfister, L., and Fuelberg, H. E.: Characteristics of the atmospheric CO₂ signal as observed over the conterminous United States during INTEX-NA, *J. Geophys. Res.-Atmos.*, 113, D07301, <https://doi.org/10.1029/2007JD008899>, 2008.
- Ciais, P., Rayner, P., Chevallier, F., Bousquet, P., Logan, M., Peylin, P., and Ramonet, M.: Atmospheric inversions for estimating CO₂ fluxes: methods and perspectives, *Climatic Change*, 103, 69–92, 2010.
- Crevoisier, C., Sweeney, C., Gloor, M., Sarmiento, J. L., and Tans, P. P.: Regional US carbon sinks from three-dimensional atmospheric CO₂ sampling, *P. Natl. Acad. Sci. USA*, 107, 18348–18353, 2010.
- Crisp, D., Fisher, B. M., O'Dell, C., Frankenberg, C., Basilio, R., Bösch, H., Brown, L. R., Castano, R., Connor, B., Deutscher, N. M., Eldering, A., Griffith, D., Gunson, M., Kuze, A., Mandrake, L., McDuffie, J., Messerschmidt, J., Miller, C. E., Morino, I., Natraj, V., Notholt, J., O'Brien, D. M., Oyafuso, F., Polonsky, I., Robinson, J., Salawitch, R., Sherlock, V., Smyth, M., Suto, H., Taylor, T. E., Thompson, D. R., Wennberg, P. O., Wunch, D., and Yung, Y. L.: The ACOS CO₂ retrieval algorithm – Part II: Global XCO₂ data characterization, *Atmos. Meas. Tech.*, 5, 687–707, <https://doi.org/10.5194/amt-5-687-2012>, 2012.
- Denning, A. S., Takahashi, T., and Friedlingstein, P.: Can a strong atmospheric CO₂ rectifier effect be reconciled with a “reasonable” carbon budget?, *Tellus B*, 51, 249–253, 1999.
- Feng, L., Palmer, P. I., Parker, R. J., Deutscher, N. M., Feist, D. G., Kivi, R., Morino, I., and Sussmann, R.: Estimates of European uptake of CO₂ inferred from GOSAT XCO₂ retrievals: sensitivity to measurement bias inside and outside Europe, *Atmos. Chem. Phys.*, 16, 1289–1302, <https://doi.org/10.5194/acp-16-1289-2016>, 2016.
- Frankenberg, C., Kulawik, S. S., Wofsy, S. C., Chevallier, F., Daube, B., Kort, E. A., O'Dell, C., Olsen, E. T., and Osterman, G.: Using airborne HIAPER Pole-to-Pole Observations (HIPPO) to evaluate model and remote sensing estimates of atmospheric carbon dioxide, *Atmos. Chem. Phys.*, 16, 7867–7878, <https://doi.org/10.5194/acp-16-7867-2016>, 2016.
- Gerbig, C., Lin, J. C., Wofsy, S. C., Daube, B. C., Andrews, A. E., Stephens, B. B., Bakwin, P. S., and Grainger, C. A.: Toward constraining regional-scale fluxes of CO₂ with atmospheric observations over a continent: 1. Observed spatial variability from airborne platforms, *J. Geophys. Res.-Atmos.*, 108, 2156–2202, <https://doi.org/10.1029/2002JD003018>, 2003.
- Gurney, K. R., Law, R. M., Denning, A. S., Rayner, P. J., Baker, D., Bousquet, P., Bruhwiler, L., Chen, Y. H., Ciais, P., Fan, S., Fung, I. Y., Gloor, M., Heimann, M., Higuchi, K., John, J., Maki, T., Maksyutov, S., Masarie, K., Peylin, P., Prather, M., Pak, B. C., Randerson, J., Sarmiento, J., Taguchi, S., Takahashi, T., and Yuen, C. W.: Towards robust regional estimates of CO₂ sources and sinks using atmospheric transport models, *Nature*, 415, 626–630, 2002.
- Gurney, K. R., Law, R. M., Denning, A. S., Rayner, P. J., Pak, B. C., Baker, D., Bousquet, P., Bruhwiler, L., Chen, Y. H., Ciais, P., Fung, I. Y., Heimann, M., John, J., Maki, T., Maksyutov, S., Peylin, P., Prather, M., and Taguchi, S.: Transcom 3 inversion intercomparison: Model mean results for the estimation of seasonal carbon sources and sinks, *Global Biogeochem. Cy.*, 18, GB1010, <https://doi.org/10.1029/2003GB002111>, 2004.
- Houweling, S., Breon, F.-M., Aben, I., Rödenbeck, C., Gloor, M., Heimann, M., and Ciais, P.: Inverse modeling of CO₂ sources and sinks using satellite data: a synthetic inter-comparison of measurement techniques and their performance as a function of space and time, *Atmos. Chem. Phys.*, 4, 523–538, <https://doi.org/10.5194/acp-4-523-2004>, 2004.
- Inoue, M., Morino, I., Uchino, O., Miyamoto, Y., Yoshida, Y., Yokota, T., Machida, T., Sawa, Y., Matsueda, H., Sweeney, C., Tans, P. P., Andrews, A. E., Biraud, S. C., Tanaka, T., Kawakami, S., and Patra, P. K.: Validation of XCO₂ derived from SWIR spectra of GOSAT TANSO-FTS with aircraft measurement data, *Atmos. Chem. Phys.*, 13, 9771–9788, <https://doi.org/10.5194/acp-13-9771-2013>, 2013.
- Inoue, M., Morino, I., Uchino, O., Nakatsuru, T., Yoshida, Y., Yokota, T., Wunch, D., Wennberg, P. O., Roehl, C. M., Griffith, D. W. T., Velasco, V. A., Deutscher, N. M., Warneke, T., Notholt, J., Robinson, J., Sherlock, V., Hase, F., Blumenstock, T., Rettinger, M., Sussmann, R., Kyrö, E., Kivi, R., Shiomi, K., Kawakami, S., De Mazière, M., Arnold, S. G., Feist, D. G., Barrow, E. A., Barney, J., Dubey, M., Schneider, M., Iraci, L. T., Podolske, J. R., Hillyard, P. W., Machida, T., Sawa, Y., Tsuboi, K., Matsueda, H., Sweeney, C., Tans, P. P., Andrews, A. E., Biraud, S. C., Fukuyama, Y., Pittman, J. V., Kort, E. A., and Tanaka, T.: Bias corrections of GOSAT SWIR XCO₂ and XCH₄ with TC-CON data and their evaluation using aircraft measurement data, *Atmos. Meas. Tech.*, 9, 3491–3512, <https://doi.org/10.5194/amt-9-3491-2016>, 2016.
- Karion, A., Sweeney, C., Tans, P., and Newberger, T.: AirCore: An Innovative Atmospheric Sampling System, *J. Atmos. Ocean. Tech.*, 27, 1839–1853, <https://doi.org/10.1175/2010JTECHA1448.1>, 2010.
- Keeling, C. D. and Rakestraw, N. W.: The concentration of carbon dioxide in the atmosphere, *J. Geophys. Res.*, 65, 2502–2502, 1960.
- Keppel-Aleks, G., Wennberg, P. O., Washenfelder, R. A., Wunch, D., Schneider, T., Toon, G. C., Andres, R. J., Blavier, J.-F., Connor, B., Davis, K. J., Desai, A. R., Messerschmidt, J., Notholt, J., Roehl, C. M., Sherlock, V., Stephens, B. B., Vay, S. A., and Wofsy, S. C.: The imprint of surface fluxes and transport on variations in total column carbon dioxide, *Biogeosciences*, 9, 875–891, <https://doi.org/10.5194/bg-9-875-2012>, 2012.
- Kulawik, S. S., Worden, J. R., Wofsy, S. C., Biraud, S. C., Nassar, R., Jones, D. B. A., Olsen, E. T., Jimenez, R., Park, S., Santoni, G. W., Daube, B. C., Pittman, J. V., Stephens, B. B., Kort, E. A., Osterman, G. B., and TES team: Comparison of improved Aura Tropospheric Emission Spectrometer CO₂ with HIPPO and SGP aircraft profile measurements, *Atmos. Chem. Phys.*, 13, 3205–3225, <https://doi.org/10.5194/acp-13-3205-2013>, 2013.
- Machida, T., Kita, K., Kondo, Y., Blake, D., Kawakami, S., Inoue, G., and Ogawa, T.: Vertical and meridional distributions of the

- atmospheric CO₂ mixing ratio between northern midlatitudes and southern subtropics, *J. Geophys. Res.-Atmos.*, 108, 8401, <https://doi.org/10.1029/2001JD000910>, 2002.
- Machida, T., Matsueda, H., Sawa, Y., Nakagawa, Y., Hirokuni, K., Kondo, N., Goto, K., Nakazawa, T., Ishikawa, K., and Ogawa, T.: Worldwide Measurements of Atmospheric CO₂ and Other Trace Gas Species Using Commercial Airlines, *J. Atmos. Ocean. Tech.*, 25, 1744–1754, 2008.
- Mesinger, F., DiMego, G., Kalnay, E., Mitchell, K., Shafran, P. C., Ebisuzaki, W., Jovic, D., Woollen, J., Rogers, E., Berbery, E. H., Ek, M. B., Fan, Y., Grumbine, R., Higgins, W., Li, H., Lin, Y., Manikin, G., Parrish, D., and Shi, W.: North American regional reanalysis, *B. Am. Meteorol. Soc.*, 87, 343–360, <https://doi.org/10.1175/BAMS-87-3-343>, 2006.
- Messerschmidt, J., Geibel, M. C., Blumenstock, T., Chen, H., Deutscher, N. M., Engel, A., Feist, D. G., Gerbig, C., Gisi, M., Hase, F., Katrynski, K., Kolle, O., Lavric, J. V., Notholt, J., Palm, M., Ramonet, M., Rettinger, M., Schmidt, M., Sussmann, R., Toon, G. C., Truong, F., Warneke, T., Wennberg, P. O., Wunch, D., and Xueref-Remy, I.: Calibration of TCCON column-averaged CO₂: the first aircraft campaign over European TCCON sites, *Atmos. Chem. Phys.*, 11, 10765–10777, <https://doi.org/10.5194/acp-11-10765-2011>, 2011.
- Miller, C. E., Crisp, D., DeCola, P. L., Olsen, S. C., Rander-son, J. T., Michalak, A. M., Alkhaled, A., Rayner, P., Jacob, D. J., Suntharalingam, P., Jones, D. B. A., Denning, A. S., Nicholls, M. E., Doney, S. C., Pawson, S., Boesch, H., Connor, B. J., Fung, I. Y., O'Brien, D., Salawitch, R. J., Sander, S. P., Sen, B., Tans, P., Toon, G. C., Wennberg, P. O., Wofsy, S. C., Yung, Y. L., and Law, R. M.: Precision requirements for space-based X-CO₂ data, *J. Geophys. Res.-Atmos.*, 112, D10314, <https://doi.org/10.1029/2006JD007659>, 2007.
- Miller, J. B., Lehman, S. J., Montzka, S. A., Sweeney, C., Miller, B. R., Karion, A., Wolak, C., Dlugokencky, J., Southon, J., Turnbull, J. C., and Tans, P. P.: Linking emissions of fossil fuel CO₂ and other anthropogenic trace gases using atmospheric 14CO₂, *J. Geophys. Res.*, 117, D08302, <https://doi.org/10.1029/2011JD017048>, 2012.
- Miller, S. T. K., Keim, B. D., Talbot, R. W., and Mao, H.: Sea breeze: Structure, forecasting, and impacts, *Rev. Geophys.*, 41, 1011, <https://doi.org/10.1029/2003RG000124>, 2003.
- Miyamoto, Y., Inoue, M., Morino, I., Uchino, O., Yokota, T., Machida, T., Sawa, Y., Matsueda, H., Sweeney, C., Tans, P. P., Andrews, A. E., and Patra, P. K.: Atmospheric column-averaged mole fractions of carbon dioxide at 53 aircraft measurement sites, *Atmos. Chem. Phys.*, 13, 5265–5275, <https://doi.org/10.5194/acp-13-5265-2013>, 2013.
- National Oceanic & Atmospheric Administration (NOAA): CarbonTracker CT2015, available at: <https://www.esrl.noaa.gov/gmd/ccgg/carbontracker/CT2015/> (last access: 18 December 2017), 2015.
- National Oceanic & Atmospheric Administration (NOAA): Observation Package (ObsPack) Data Products, available at: <https://doi.org/10.15138/G3H59M> (last access: 18 December 2017), 2016.
- Sweeney, C., Newberger, T., Wolter, S., Chen, H., Fischer, M. L., Higgs, J., and Lan, X.: AirCore data in the study of “Gradients of column CO₂ across North America from the NOAA Global Greenhouse Gas Reference Network”, available at: <https://doi.org/10.15138/G3N33W>, last access: 18 December 2017.
- Peters, W., Jacobson, A. R., Sweeney, C., Andrews, A. E., Conway, T. J., Masarie, K., Miller, J. B., Bruhwiler, L. M. P., Petron, G., Hirsch, A. I., Worthy, D. E. J., van der Werf, G. R., Randerson, J. T., Wennberg, P. O., Krol, M. C., and Tans, P. P.: An atmospheric perspective on North American carbon dioxide exchange: CarbonTracker, *P. Natl. Acad. Sci. USA*, 104, 18925–18930, 2007.
- Ramonet, M., Ciais, P., Nepomniachii, I., Sidorov, K., Neubert, R. E. M., Langendorfer, U., Picard, D., Kazan, V., Biraud, S., Gusti, M., Kolle, O., Schulze, E. D., and Lloyd, J.: Three years of aircraft-based trace gas measurements over the Fyodorovskoye southern taiga forest, 300 km north-west of Moscow, *Tellus B*, 54, 713–734, 2002.
- Reuter, M., Bovensmann, H., Buchwitz, M., Burrows, J. P., Connor, B. J., Deutscher, N. M., Griffith, D. W. T., Heymann, J., Keppel-Aleks, G., Messerschmidt, J., Notholt, J., Petri, C., Robinson, J., Schneising, O., Sherlock, V., Velasco, V., Warneke, T., Wennberg, P. O., and Wunch, D.: Retrieval of atmospheric CO₂ with enhanced accuracy and precision from SCIAMACHY: Validation with FTS measurements and comparison with model results, *J. Geophys. Res.-Atmos.*, 116, D04301, <https://doi.org/10.1029/2010JD015047>, 2011.
- Reuter, M., Buchwitz, M., Hilker, M., Heymann, J., Schneising, O., Pillai, D., Bovensmann, H., Burrows, J. P., Bösch, H., Parker, R., Butz, A., Hasekamp, O., O'Dell, C. W., Yoshida, Y., Gerbig, C., Nehr Korn, T., Deutscher, N. M., Warneke, T., Notholt, J., Hase, F., Kivi, R., Sussmann, R., Machida, T., Matsueda, H., and Sawa, Y.: Satellite-inferred European carbon sink larger than expected, *Atmos. Chem. Phys.*, 14, 13739–13753, <https://doi.org/10.5194/acp-14-13739-2014>, 2014.
- Reuter, M., Buchwitz, M., Hilker, M., Heymann, J., Bovensmann, H., Burrows, J. P., Houweling, S., Liu, Y. Y., Nassar, F., Chevalier, F., Ciais, P., Marshall, J., and Reichstein, M.: How much CO₂ is taken up by the European terrestrial biosphere?, *B. Am. Meteorol. Soc.*, 98, 665–671, <https://doi.org/10.1175/BAMS-D-15-00310.1>, 2017.
- Saitoh, N., Kimoto, S., Sugimura, R., Imasu, R., Kawakami, S., Shiomi, K., Kuze, A., Machida, T., Sawa, Y., and Matsueda, H.: Algorithm update of the GOSAT/TANSO-FTS thermal infrared CO₂ product (version 1) and validation of the UTLS CO₂ data using CONTRAIL measurements, *Atmos. Meas. Tech.*, 9, 2119–2134, <https://doi.org/10.5194/amt-9-2119-2016>, 2016.
- Stephens, B. B., Gurney, K. R., Tans, P. P., Sweeney, C., Peters, W., Bruhwiler, L., Ciais, P., Ramonet, M., Bousquet, P., Nakazawa, T., Aoki, S., Machida, T., Inoue, G., Vinnichenko, N., Lloyd, J., Jordan, A., Heimann, M., Shibistova, O., Langenfelds, R. L., Steele, L. P., Francey, R. J., and Denning, A. S.: Weak northern and strong tropical land carbon uptake from vertical profiles of atmospheric CO₂, *Science*, 316, 1732–1735, 2007.
- Sweeney, C., Karion, A., Wolter, S., Newberger, T., Guenther, D., Higgs, J. A., Andrews, A. E., Lang, P. M., Neff, D., Dlugokencky, E., Miller, J. B., Montzka, S. A., Miller, B. R., Masarie, K. A., Biraud, S. C., Novelli, P. C., Crotwell, M., Crotwell, A. M., Thoning, K., and Tans, P. P.: Seasonal climatology of CO₂ across North America from aircraft measurements in the NOAA/ESRL Global Greenhouse Gas Reference Network, *J. Geophys. Res.-Atmos.*, 120, 5155–5190, 2015.

- Tanaka, M., Nakazawa, T., and Aoki, S.: Concentration of atmospheric carbon-dioxide over Japan. *J. Geophys. Res.-Oceans*, 88, 1339–1344, <https://doi.org/10.1029/JC088iC02p01339>, 1983.
- Tanaka, T., Miyamoto, Y., Morino, I., Machida, T., Nagahama, T., Sawa, Y., Matsueda, H., Wunch, D., Kawakami, S., and Uchino, O.: Aircraft measurements of carbon dioxide and methane for the calibration of ground-based high-resolution Fourier Transform Spectrometers and a comparison to GOSAT data measured over Tsukuba and Moshiri. *Atmos. Meas. Tech.*, 5, 2003–2012, <https://doi.org/10.5194/amt-5-2003-2012>, 2012.
- Tans, P. P., Conway, T. J., and Nakazawa, T.: Latitudinal distribution of the sources and sinks of atmospheric carbon-dioxide derived from surface observations and an atmospheric transport model. *J. Geophys. Res.-Atmos.*, 94, 5151–5172, 1989.
- Tans, P. P., Fung, I. Y., and Takahashi, T.: Observational constraints on the global atmospheric CO₂ budget. *Science*, 247, 1431–1438, 1990.
- Thoning, K. W., Tans, P. P., and Komhyr, W. D.: Atmospheric carbon-dioxide at Mauna Loa observatory. 2. Analysis of the NOAA GMCC data, 1974–1985. *J. Geophys. Res.-Atmos.*, 94, 8549–8565, 1989.
- Washenfelder, R. A., Toon, G. C., Blavier, J. F., Yang, Z., Allen, N. T., Wennberg, P. O., Vay, S. A., Matross, D. M., and Daube, B. C.: Carbon dioxide column abundances at the Wisconsin Tall Tower site. *J. Geophys. Res.-Atmos.*, 111, D22305, <https://doi.org/10.1029/2006JD007154>, 2006.
- Wofsy, S. C.: HIAPER Pole-to-Pole Observations (HIPPO): fine-grained, global-scale measurements of climatically important atmospheric gases and aerosols. *Philos. T. Roy. Soc. A*, 369, 2073–2086, <https://doi.org/10.1098/rsta.2010.0313>, 2011.
- Wunch, D., Wennberg, P. O., Toon, G. C., Keppel-Aleks, G., and Yavin, Y. G.: Emissions of greenhouse gases from a North American megacity. *Geophys. Res. Lett.*, 36, L15810, <https://doi.org/10.1029/2009GL039825>, 2009.
- Wunch, D., Toon, G. C., Wennberg, P. O., Wofsy, S. C., Stephens, B. B., Fischer, M. L., Uchino, O., Abshire, J. B., Bernath, P., Biraud, S. C., Blavier, J.-F. L., Boone, C., Bowman, K. P., Browell, E. V., Campos, T., Connor, B. J., Daube, B. C., Deutscher, N. M., Diao, M., Elkins, J. W., Gerbig, C., Gottlieb, E., Griffith, D. W. T., Hurst, D. F., Jiménez, R., Keppel-Aleks, G., Kort, E. A., Macatangay, R., Machida, T., Matsueda, H., Moore, F., Morino, I., Park, S., Robinson, J., Roehl, C. M., Sawa, Y., Sherlock, V., Sweeney, C., Tanaka, T., and Zondlo, M. A.: Calibration of the Total Carbon Column Observing Network using aircraft profile data. *Atmos. Meas. Tech.*, 3, 1351–1362, <https://doi.org/10.5194/amt-3-1351-2010>, 2010.
- Wunch, D., Toon, G. C., Blavier, J.-F. L., Washenfelder, R. A., Notholt, J., Connor, B. J., Griffith, D. W. T., Sherlock, V., and Wennberg, P. O.: The total carbon column observing network. *Philos. T. Roy. Soc. A*, 369, 2087–2112, <https://doi.org/10.1098/rsta.2010.0240>, 2011.
- Wunch, D., Wennberg, P. O., Messerschmidt, J., Parazoo, N. C., Toon, G. C., Deutscher, N. M., Keppel-Aleks, G., Roehl, C. M., Randerson, J. T., Warneke, T., and Notholt, J.: The covariation of Northern Hemisphere summertime CO₂ with surface temperature in boreal regions. *Atmos. Chem. Phys.*, 13, 9447–9459, <https://doi.org/10.5194/acp-13-9447-2013>, 2013.
- Wunch, D., Wennberg, P. O., Osterman, G., Fisher, B., Naylor, B., Roehl, C. M., O'Dell, C., Mandrake, L., Viatte, C., Kiel, M., Griffith, D. W. T., Deutscher, N. M., Velasco, V. A., Notholt, J., Warneke, T., Petri, C., De Maziere, M., Sha, M. K., Sussmann, R., Rettinger, M., Pollard, D., Robinson, J., Morino, I., Uchino, O., Hase, F., Blumenstock, T., Feist, D. G., Arnold, S. G., Strong, K., Mendonca, J., Kivi, R., Heikkinen, P., Iraci, L., Podolske, J., Hillyard, P. W., Kawakami, S., Dubey, M. K., Parker, H. A., Sepulveda, E., García, O. E., Te, Y., Jeseck, P., Gunson, M. R., Crisp, D., and Eldering, A.: Comparisons of the Orbiting Carbon Observatory-2 (OCO-2) X_{CO₂} measurements with TCCON. *Atmos. Meas. Tech.*, 10, 2209–2238, <https://doi.org/10.5194/amt-10-2209-2017>, 2017.